Journal of
Microscopy

*Journal of Microscopy, Vol. 246, Pt 1 2012, pp. 60–69*
*Received 17 August 2011; accepted 30 November 2011*

doi: 10.1111/j.1365-2818.2011.03587.x

# Cryo-SEM specimen preparation under controlled temperature and concentration conditions

L. ISSMAN & Y. TALMON
*Department of Chemical Engineering, Russell Berrie Nanotechnology Institute (RBNI), Technion-Israel Institute of Technology, Haifa, Israel*

**Key words.** Carbon nanotubes, controlled environment vitrification system, Cryo-SEM, microemulsions, specimen preparation.

## Summary

Cryogenic temperature scanning electron microscopy (cryo-SEM) is an excellent technique for imaging liquid and semi-liquid materials of high vapour pressure, which are highly viscous or contain large (>0.5 $\mu$m) aggregates, in which nanometric details are to be studied. However, so far there have been no adequate tools for controlled cryo-specimen preparation. The specimen preparation stage is critical, because most of those samples are very sensitive to concentration and temperature changes, leading to nanostructural artefacts in the specimens. We designed and built a system for easy and reliable cryo-SEM specimen preparation under controlled conditions of fixed temperature and humidity. We describe this new methodology, and demonstrate its applicability, by showing imaging data of three liquid material systems. We have studied carbon nanotubes (CNTs) dispersions in superacid. We also characterized a number of systems made of water/isooctane/nonionic and cationic surfactant that showed different microemulsion phases as function of the system composition and temperature. In all of the examples given, we demonstrate artefact- and contamination-free specimens, which have preserved their native nanostructure. Our new system paves the way for a new methodology for the newly emerging field of cryo-SEM.

## Introduction

Electron microscopy (EM) at cryogenic temperatures is used for high-resolution imaging of high vapour-pressure specimens. These samples are aqueous or nonaqueous systems, such as gels, suspensions, emulsions or biological specimens and even solids of high vapour pressure. One needs cryogenic conditions to avoid loss of volatiles from the specimen in the high vacuum of the EM. Sufficiently low temperatures reduce the vapour pressure to negligible levels. Also, those conditions suppress motion on the supramolecular level, which could lead to blurry images. Fast enough cooling vitrifies the specimen, thus preserving its nanostructure (Costello *et al.*, 1982; Elder *et al.*, 1982). Nevertheless, one must remember that when dealing with pure water or low concentration solutions, a thin film of less than 1 $\mu$m can be actually vitrified. Cryo-EM provides high-resolution direct images in a wide range of domain sizes, from a few nanometres to tens of microns. This helps understanding the nature of the basic building blocks of the studied system. As such systems often include different coexisting assembly types, cryo-EM allows observing them all, even those which are hard to tell apart and identify by other indirect methods such as scattering techniques. Data interpretation from cryo-EM is often straightforward, not model dependent, whereas, data interpretation from indirect methods, is quite complicated in complex systems containing more than one aggregate type or a broad size distribution.

Thermal fixation by rapid cooling, rather than chemical fixation, is a preferable technique for fixing labile specimens (Talmon *et al.*, 1979). The thin-film vitrification method pioneered by Dubochet *et al.* (Adrian *et al.*, 1984) has proven itself successful in preparing specimens for transmission electron microscopy at cryogenic temperatures (cryo-TEM). Although, cryo-TEM has become an important direct-imaging method, it cannot be used for highly viscous samples or those containing large objects, as the specimens must be very thin (100–300 nm thick) and larger objects are excluded from the specimen during preparation (Talmon, 2007).

Cryo-SEM gives images showing the macro-, micro- and even nanostructure in the imaged sample. It provides 3D like topographical details of the sample surface, because of its unique image acquisition method and depth of field. The cryo-SEM method was first suggested already in the 1970s (Echlin *et al.*, 1970), however published high-resolution data of labile or reactive systems by this technique is sparse. The main reason for the limited resolution has been lack

Correspondence to: Y. Talmon, Department of Chemical Engineering, The Russell Berrie Nanotechnology Institute (RBNI), Technion-Israel Institute of Technology, Haifa 32000, Israel. Tel: +972–4-8292007; fax: +972-1534-8242617; e-mail: ishi@tx.technion.ac.il

of appropriate hardware. However, in recent years much progress in SEM technology has been made, especially through improved field emission guns (FEGs), column design and modern detectors, allowing high-resolution imaging, down to the nanoscale (Jaksch *et al.*, 2005; Wandrol, 2007). Those improvements mainly affected standard SEM imaging of room-temperature solid specimens. To perform cryo-SEM on those improved microscopes one needs well-controlled conditions during specimen preparation and transfer into the liquid nitrogen ($LN_2$) cooled SEM cryo-specimen holder. Cryo-SEM attachments have been offered by a number of vendors (Wepf *et al.*, 2004), but there are almost no systems that offer proper conditions for specimen preparation. Properly controlled specimen preparation is critical, because most specimen artefacts are formed at that stage. Because many of the material systems examined by cryo-SEM are very sensitive to temperature and composition changes, temperature and saturation of the gas phase surrounding the specimen must be controlled and remain steady during the preparation procedure, until complete thermal fixation of the specimen.

A number of techniques have been developed and used to vitrify specimens. These include, for example, cryo-jet spray fracturing (Knoll *et al.*, 1982), cold block cryo-fixation (Hisada *et al.*, 2001) and high-pressure freeze fracturing which was first conceived and later developed by Moor & Riehle (1968); Moor (1987) and is widely used today (Walther, 2003; Osumi *et al.*, 2006; Taribagil *et al.*, 2010). However, none of those techniques offer controlled conditions before or during specimen preparation until thermal fixation. In addition, the high-pressure freeze fracturing method, although effective, uses in most cases alcohol as a pressure transducing liquid. Even small amounts of alcohol could alter the nanostructure of a microemulsion, for example. However, that much of the data acquired by those systems seem artefact-free is probably because most of the systems studied by that methodology have been biological systems, many of which not very sensitive to ambient conditions. However, complex nanostructured liquids change readily upon changes in temperature and concentration and thus require better control of ambient conditions around the prepared specimen to prevent nanostructural artefacts. The specimen preparation system that was developed by Ge *et al.* (2007) does include a controlled environment, however, it was not designed for specimens that are to be fractured, but for imaging the specimen surface, as in the study of coatings.

As in the former case, our system is based on the controlled environment vitrification system (CEVS) introduced by Bellare *et al.* (1986, 1988), which was further modified by Talmon (1996). This system has been successfully applied to prepare cryo-TEM vitrified specimens of a wide range of complex liquids for more than 25 years (e.g. Miller *et al.*, 1987; Zheng *et al.*, 1999; Koh *et al.*, 2010). We have modified the CEVS system to allow us prepare cryo-SEM specimens under controlled conditions. The same system may be used similarly to prepare freeze-fracture replicas (Omer *et al.*, 2009). The procedure is based on the preparation of a liquid sample sandwiched between two gold planchettes, namely small round shallow receptacles, made of gold (Fig. 1). The assembled sandwich is plunged into a cryogen and transferred into a BAF060 unit (BAL-TEC AG, Balzers, Liechtenstein), where it is opened under vacuum and cryogenic temperature, thus producing two fracture surfaces. Then the surface may be coated and the specimen is transferred to the cryo-stage of the SEM. Alternatively, freeze-fracture replicas are made of the fracture surfaces.

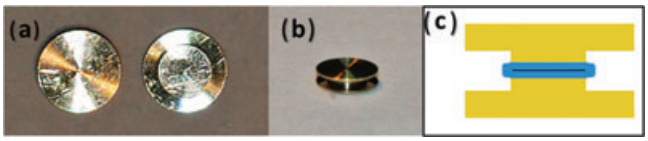


**Fig. 1.** Images of the golden specimen carriers. (a) Upper and lower planchettes; (b) assembled sandwich; (c) cross-section schematic of an assembled sandwich.

Here we report the design of the new CEVS and the methodology of cryo-SEM specimen preparation with it. We then give several examples of preparing artefact-free specimens for high-resolution cryo-SEM.

## Instrumentation

### *Instrument design*

Fig. 2 shows the new CEVS, which consists of four modules: (1) temperature control module, (2) environmental chamber, (3) plunge module and (4) cryogen box.

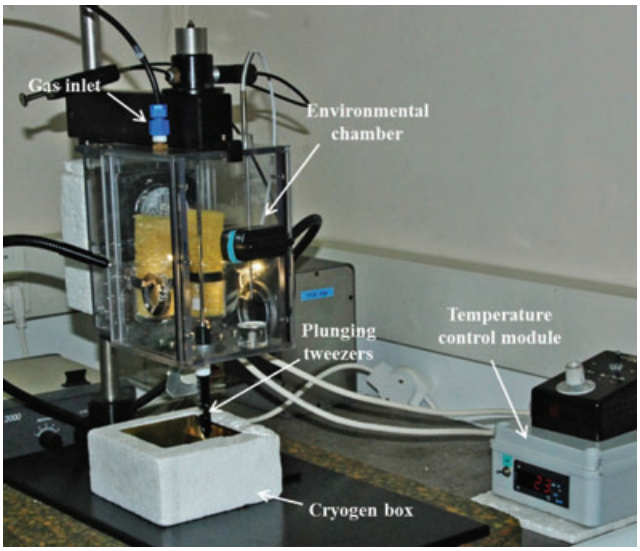


**Fig. 2.** Overview of the CEVS. The tweezers are shown in the plunged position inside the cryogen box.

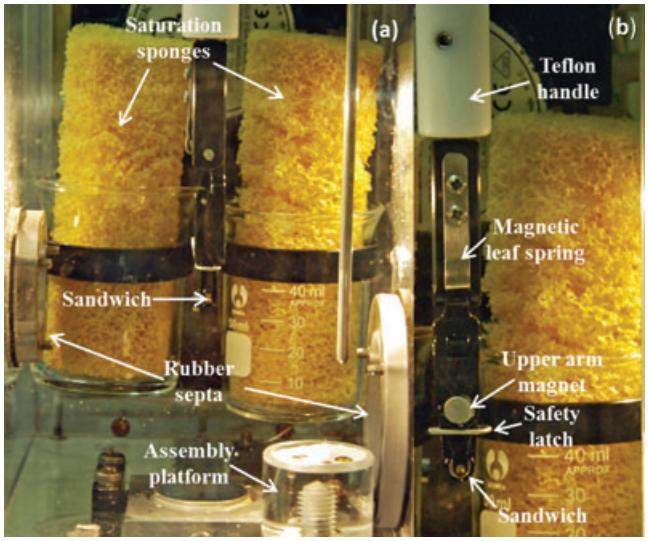


**Fig. 3.** The inner part of the environmental chamber. The tweezers are at the vertical mode, latch on and prior plunging. (a) Tweezers side-view; (b) tweezers on-view.

*Temperature and humidity control module*. This module of the CEVS was left as in the original design. The chamber is heated by a high-power light bulb, controlled by an on-off controller and a manual rheostat. The gas-phase saturation in the chamber is maintained by two sponges containing the volatile liquids with which the gas phase is saturated. A small fan circulates the air over the sponges to minimize relative humidity and temperature gradients.

*Environmental chamber*. The environmental chamber has basically the same design of the original CEVS, but with some modifications. The polycarbonate chamber is $10 \times 10 \times 20\ cm^3$. The front wall and two sidewalls are one separate unit, sliding in and out from the rest of the chamber, when the CEVS is readied for specimen preparation. Specimen manipulation is performed through two rubber septa located on the sidewalls. On the lower left part of the right wall, a bigger septum (4 cm in diameter) was installed to facilitate specimen preparation. A small platform on the chamber floor covered with a replaceable filter paper sheet has been added (Fig. 3a). Sandwich assembly is conducted on that platform. This allows the planchettes and EM grids to be kept inside the chamber in equilibrium with their surroundings. A gas inlet was also added to the chamber ceiling. This is used when specimen preparation is to be carried out in an atmosphere of dry inert gas, e.g. dry nitrogen.

*Plunging module*. The new plunging module, as the former one, is mounted on a spring-loaded plunger. Here we use a new type of 'tweezers' that hold the sandwiched specimen. The tweezers need to be small enough to fit into the CEVS chamber. Moreover, the small size of the tweezers also makes it possible to easily rotate them from the horizontal to the vertical position (Fig. 4a). The tweezers are locked in a specific position by a leaf spring-socket mechanism (see arrow in Fig. 4b). The user prepares the specimen in the CEVS, while the tweezers are in the horizontal position. To ease this procedure, the leaf spring is magnetic, so that the upper tweezers arm is locked in place, while the sandwich is assembled (Fig. 5a). Plunging in the vertical position maximizes heat transfer and minimizes shear stress and splashing upon contact with the cryogen. Two small and powerful magnets are fixed in each of the arms to tightly lock the tweezers around the specimen. In addition to the magnets, a safety-latch has been added to firmly lock the tweezers and to prevent their accidental opening during the plunging (Fig. 3b). The safety-latch is very easily inserted in place, as it is magnetized and attaches itself near the magnets. It is removed easily after plunging. A white Teflon handle was fixed on the tweezers neck (Fig. 3b) for thermal insulation, which helps manipulate the tweezers while they are still immersed in the cryogen. Also, we added at the bottom of the tweezers lower arm a small hole (Fig. 6c), used to push out a sandwich, still immersed in the cryogen, if it is stuck in the tweezers.

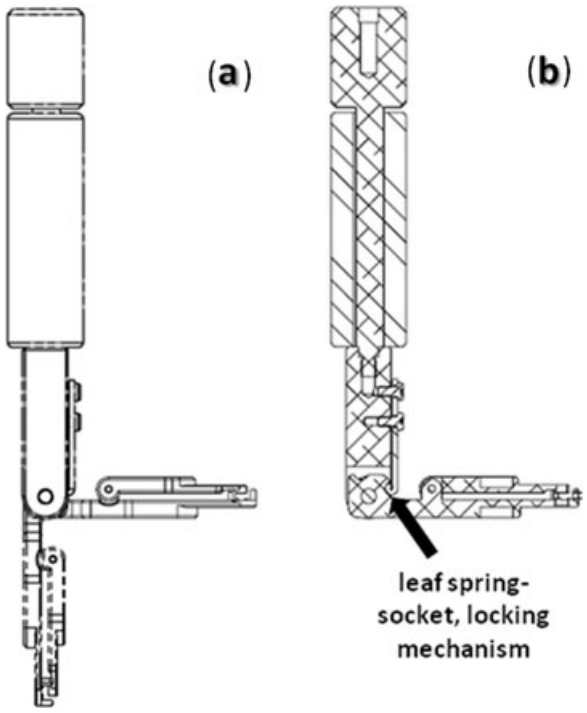


**Fig. 4.** Drawings of the CEVS tweezers. (a) Tweezers side-view showing two optional working modes; (b) tweezers cross-section showing locking mechanism.

The new CEVS design allows complete manipulation of the specimen sandwich from outside the chamber and its preparation in a controlled atmosphere. It also allows to assemble the sandwich easily in the tweezers. The use of only three teeth surrounding the sandwich reduces its thermal inertia and increases direct exposure to the cryogen,

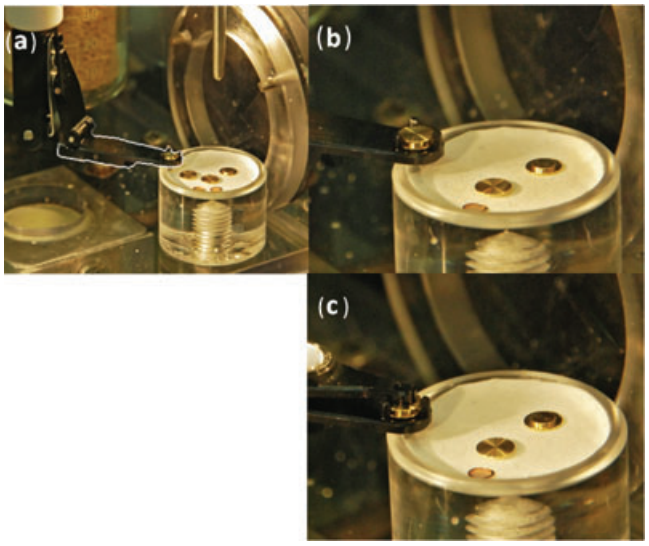


**Fig. 5.** The sandwich assembly process inside the CEVS while the tweezers (highlighted) are stationed on the small assembly platform in the horizontal position. (a) Upper arm is opened and locked because of the attraction between the magnet and stainless steel magnetic leaf spring. The lower planchette is placed in the jig whereas the others rest on the platform with the grids; (b) the sample is applied on a grid, and sandwiched between two planchettes inside the three-toothed jig; (c) the upper arm is closed gently and the tweezers arms are magnetically locked.

thus improving sample cooling. Moreover, by clamping the sandwich at its perimeter, the pressure on the planchettes and the sample is uniform and mild.

*Cryogen box*. The box holding the cryogen, liquid ethane at it freezing point for aqueous systems, $LN_2$ for nonaqueous systems (Danino *et al.*, 2002) has also been modified. The oval brass cup holding the cryogen is now wider and elongated (4 cm long and 3 cm wide; Fig. 6). This design reduces ethane splash upon specimen plunging and allows better access to open the tweezers after the plunge. It also allows resting the upper arm of the tweezers on top of the cup edges, so it does not interfere with further procedures (Fig. 6b). Also, a small storing stage has been added next to the cup (Fig. 6b), where the sandwich is kept before its insertion into the BAF060 sample table. This helps detaching any pieces of solid ethane, which may have accumulated on the sandwich surface, when it is inserted back to the $LN_2$ reservoir. The stage height is about 2 cm to ensure that a thick enough layer (more than 1 cm) of $LN_2$ always covers the sandwiches.

### *Operation*

We operate the CEVS in a fume hood, to pump away nitrogen gas and possibly small amounts of ethane vapour. We keep the room air-conditioned to 20°C to reduce the ambient humidity. The step-by-step description of the CEVS operation to prepare a cryo-SEM specimen is given below.

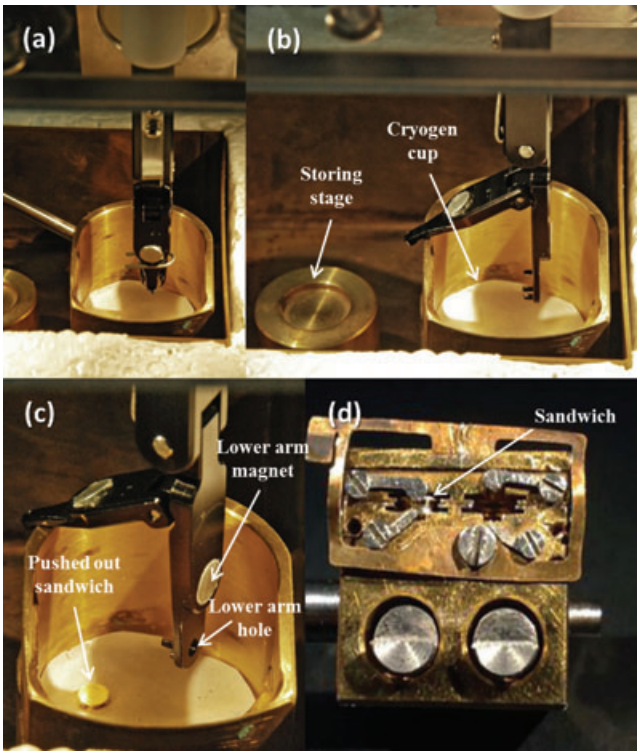


**Fig. 6.** The postplunging process (shown for clarity without a cryogen). (a) The tweezers after plunging, safety latch on; (b) the latch is removed and the tweezers are rotated 90°, upper arm is opened; (c) the sandwich is pushed out from the tweezers through the lower arm hole; (d) the sandwich is inserted into the BAL-TEC holder for double replica technique / mirror fracturing.

(1) The sliding door is opened and a fresh piece of filter paper is fixed on the small platform. Four planchettes and two copper grids are placed on the platform. The tweezers are screwed into the retracted plunging rod, locked in the horizontal mode on the platform. The upper tweezers arm is opened until it reaches the tweezers neck and is secured by the magnet and the magnetic leaf spring (Fig. 5a).
(2) Both sponges are soaked with the appropriate solvent or the sample itself and placed inside glass beakers in the rear of the chamber.
(3) The sliding door is closed and secured by the latch and so is the CEVS bottom trap door. The fan and temperature controller are switched on, the desired temperature is set and the equilibration process begins.
(4) After the temperature has reached the desired value and the chamber has become saturated, the cryogen box is filled with $LN_2$ and then the cryogen cup is fully filled with liquid ethane at its freezing point.
(5) One planchette is taken from the platform and is inserted into the lower tweezers arm between the three teeth. Approximately 3 $\mu$L of the preequilibrated sample is pipetted and applied onto the planchette.

(6) A copper grid is immersed in the sample and placed on the planchette. A second planchette is placed facedown on top of the immersed grid (Fig. 5b). The upper arm is lowered gently until it touches the sandwich and is secured by the magnets (Fig. 5c). The safety latch is inserted into the CEVS and placed on the tweezers, securing it. The tweezers are rotated away from the platform, shifted into the vertical position and locked in that position (Fig. 3).

(7) To plunge the specimen into the cryogen, we activate a cable release, opening the bottom trap door and activating the plunge mechanism. The sandwich is left immersed in the ethane for a few seconds (Fig. 6a).

(8) The upper tweezers arm is opened. The tweezers are rotated axially 90° and then the upper arm is rested on the cryogen cup edge (Fig. 6b). If the sandwich does not fall out of the tweezers, a thin metal pin is inserted through the hole in the lower arm, pushing the sandwich out (Fig. 6c).

(9) The sandwich is moved immediately from the cryogen cup into the $LN_2$ pool to be rested on the submerged small storing stage. This manoeuvre helps remove crystals of ethane that may coat the sandwich during transfer. The sandwiches are left on this stage for a couple of minutes, making sure that any pieces of ethane ice have been detached from the sandwich. This assures smooth insertion of the sandwiches into the 'sample table' (see later).

(10) The tweezers are unscrewed from the plunging shaft, removed from the chamber and the trap door is closed. All used tools are dried thoroughly to avoid ice formation on them, before the next specimen preparation. It is of utmost importance to dry the tweezers jig so the sandwich does not stick to the tweezers after the next plunging, making it almost impossible to dislodge it without destroying the specimen.

(11) After two sandwiches have been prepared as described above, they are inserted into the BAL-TEC 'sample table' for the double-replica technique/mirror fracturing (Fig. 6d). The sample table is then transferred into the BAL-TEC BAF060 for further processing. If more than two sandwiches are made, they are stored in a small cup under $LN_2$ for later inspection.

*Preparing and imaging different volatile systems with cryo-HRSEM*

To demonstrate the performance of the new CEVS, we show here its application to a number of systems. All samples were prepared as described above (with some relevant adjustments). After two sandwiches were vitrified in ethane at its freezing point, they were inserted into the BAL-TEC holder for double-replica mirror fracturing technique, while still under $LN_2$. The holder was then quickly taken into the BAL-TEC loading box, where it was loaded into the VCT100 shuttle, which keeps the specimen under vacuum and cryogenic conditions. By using the shuttle, it is possible to transfer the specimen through an airlock into the BAL-TEC BAF060 preparation unit. In this unit the specimen was fractured at –180°C. Then, to enhance topographical contrast, the specimen was heated to –100°C for 5 s, thus lightly etching its surface. Then it was coated by an electron-beam evaporator with 4 nm of Pt/C at –150°C (Fig. 7). The ready specimen was transferred by the shuttle to the $LN_2$ cooled BAL-TEC cryo-stage of the Zeiss Ultra Plus HRSEM, kept at about –145°C. The fracture surfaces were imaged at a low acceleration voltage of 1 kV, at a working distance (WD) of 3–5 mm. Most imaging has been done using the two secondary electron detectors of our SEM: either the Everhart–Thornley detector or the high-resolution in-the-column detector (SE2 and InLens detector in the Zeiss nomenclature). Quite often we used a mixture of both signals to allow high resolution and good perception of the specimen topography.

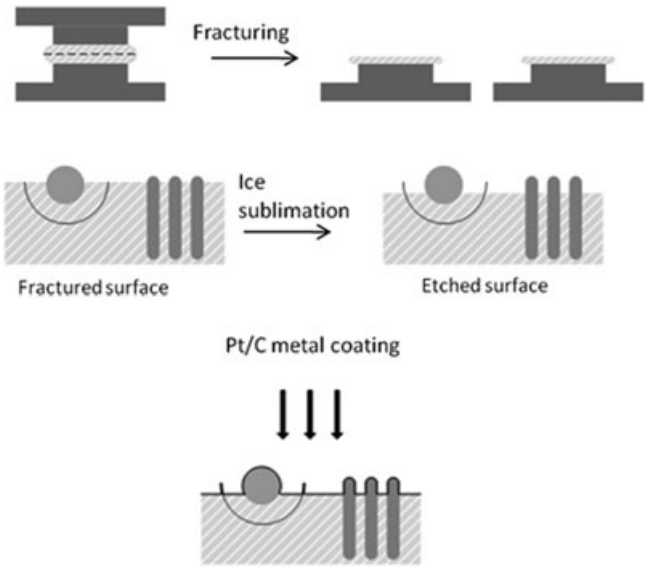


**Fig. 7.** The specimen preparation method inside the BAL-TEC BAF060 unit, after Omer *et al.* (2009).

## Results and discussion

By using the modified CEVS, it is much easier to prepare specimens than in our former method. Not only is the entire preparation, until thermal fixation, under controlled conditions, but it also takes less time, thus minimizing the risk of artefacts. Using the new CEVS also dramatically lowers the chances of the sandwich breaking up while being prepared because of the use of a jig for the sandwich assembly.

*Example #1: The microemulsion system of water-isooctane-7% wt. pentaethylene glycol monododecyl ether ($C_{12}E_5$).*

Although studies on microemulsions began in the late 1950s (Shulman *et al.*, 1959), no direct, high-resolution,

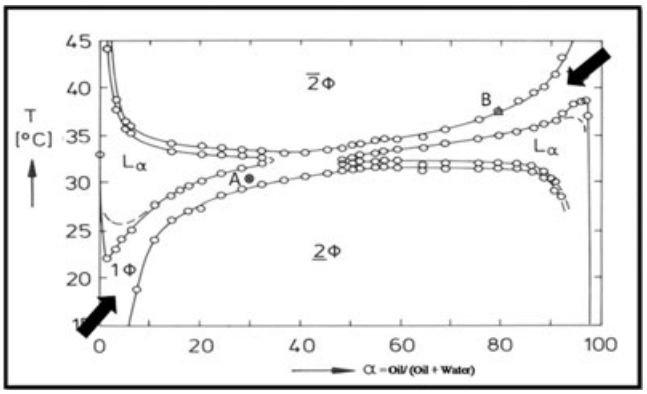


**Fig. 8.** $H_2O$-n-octane-$C_{12}E_5$ (7% wt.) pseudo binary phase-diagram including samples A and B coordinates. Arrows border the monophasic 'channel', after Kahlweit *et al.* (1987).

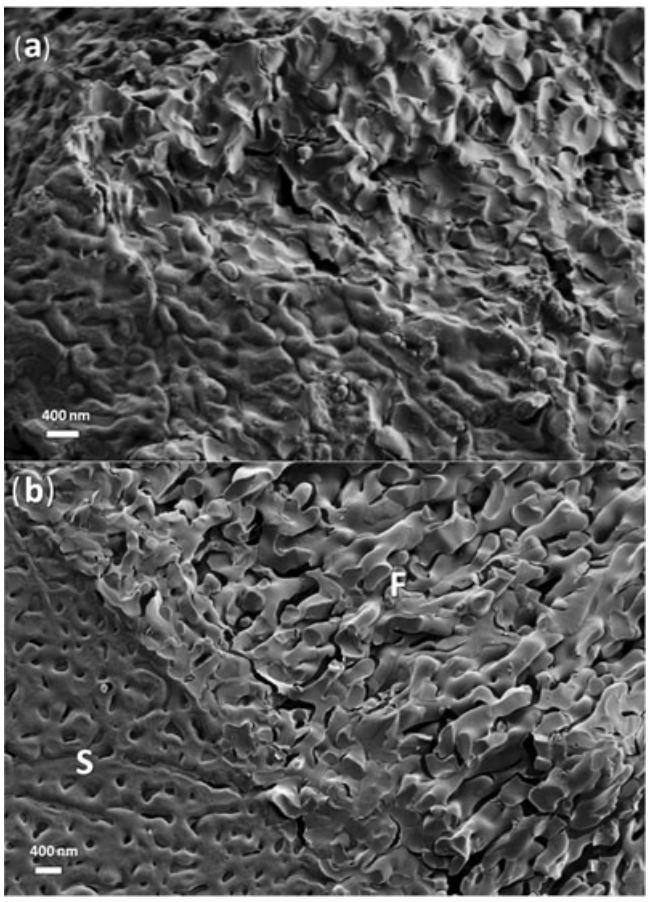


**Fig. 9.** Cryo-SEM image of the microemulsion system of $H_2O$–isooctane–7% wt.-$C_{12}E_5$ (oil fraction in the water-oil mix, $\alpha = 30\%$ wt.) at 31°C. (a) Image showing bicontinuous phase present in the specimen bulk. The image was obtained with the SE2 detector at WD of 4.9 mm; (b) image showing partially fractured specimen. S marks the specimen surface and F marks the fracture. The image was obtained with the InLens and SE2 detectors, mixed 1:1, at WD of 3 mm.

imaging data has been acquired yet. Only freeze-fracture-replication images were reported by Jahn & Strey (1988). However, those replicas were not prepared under fully controlled conditions. We are interested in the phase behaviour of the monophasic microemulsion system containing different ratios of water/isooctane with a constant concentration (7% wt.) of the nonionic surfactant $C_{12}E_5$. We especially want to follow the transitions between the different microemulsion nanostructures because of concentration and temperature modifications, while still staying in the monophasic regime. According to the pseudo binary phase diagram (Fig. 8) reported by Kahlweit *et al.* (1987), a monophasic microemulsion 'channel' exists (bordered by the two arrows) for a very similar system. Because liquid ethane, the best cryogen for specimen vitrification, cannot be used for this system as it dissolves the oil, the use of $LN_2$ as a cryogen, was imperative. However, to vitrify this specimen properly, we decided to use the branched isooctane instead of the original n-octane, because the former can be vitrified even in $LN_2$, which is a much less efficient cryogen, whereas normal hydrocarbons freeze (crystallize) in it (Danino *et al.*, 2002). No major deviations were seen from the original n-octane system, as both samples we examined seemed monophasic while still inside the 1-phase 'channel' (see A & B in Fig. 8). Sample A (oil-to-solution ratio, $\alpha = 30\%$ wt.) and B (oil-to-solution ratio, $\alpha = 80\%$ wt.) were prepared as mentioned previously, at constant temperatures of 31°C and 37°C, respectively. The CEVS was saturated by the system mixture itself and was quenched in $LN_2$. The fractured specimens were not deliberately etched. Because of the high vapour-pressure of isooctane, even at very low temperatures (NIST database after Milazzo, 1956), some sublimation did take place during specimen manipulation, without additional heating.

From the images we obtained, it is possible to see that the data was acquired from the samples bulk as the fractured specimen face is notably seen. Sample A exhibits a bicontinuous phase (Fig. 9), in agreement with what was suggested in the literature by Jahn & Strey (1988) for the n-octane system. The domains range in size of 200–300 nm. Moreover, because of the topographical contrast of the imaging method, it can clearly be seen that both domains are mutually intertwined with no drying or freezing artefacts. Images of sample B show a reverse swollen micellar phase. It can be seen that some of the particles are embedded within the isooctane continuous phase. One can infer that these nanoaggregates are indeed swollen-water micelles, as their sizes vary only between a small range of 100–200 nm, much larger than normal micelles, but too uniform in size to be small vesicles. This information also agrees with that of Jahn & Strey (1988). Although most micelles are agglomerated but still have distinct borders, fusion of some micelles is also noticeable (arrowheads in Fig. 10), probably an intermediate aggregate en-route to the bicontinuous phase. It is also possible to notice some imprint holes (arrows in Fig. 10) of micelles detached

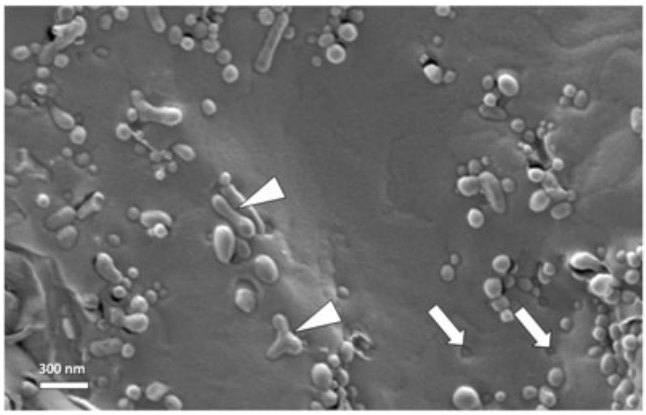


**Fig. 10.** Cryo-SEM image of the microemulsion system of $H_2O$–isooctane–7% wt. $C_{12}E_5$ (oil fraction in the water-oil mix, $\alpha = 80\%$ wt.) at 37°C. The image shows reverse, water swollen and micelles in the isooctane matrix. Arrowheads show some fused micelles most likely creating an intermediate aggregate en-route to the bicontinuous phase. Arrows show holes created as an imprint of detached micelles. The image was obtained with the InLens and SE2 detectors with a mixing ratio of 0.7:0.3 at WD of 3 mm.

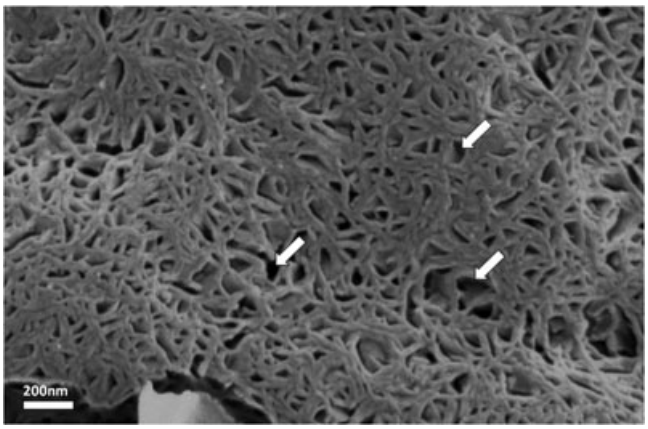


**Fig. 11.** Cryo-SEM image of the microemulsion system of $H_2O$–isooctane–DDAB (O/S = 1.5, $H_20$ 20% wt.) at 25°C. A network of water conduits intertwined with isooctane nanodomains is seen. Arrows point holes occasionally seen between the conduits, probably isooctane that got sublimated. The image was obtained with the InLens and SE2 detectors with a mixing ratio of 0.7:0.3 at WD of 3 mm.

from the specimen, as it was fractured and present in the complementary fracture surface.

We were able to image these systems by cryo-TEM, too (see Supporting information). Those data agree well with the cryo-SEM data shown here, thus supporting the success of the new methodology to preserve the nanostructure of those labile systems.

*Example #2: The microemulsion system of water-isooctane-didodecyldimethyl-ammonium bromide (DDAB) at a constant oil/surfactant (O/S) ratio of 1.5.*

Microemulsions consisting ionic surfactants have been extensively studied, producing models that predict the phase behaviour of those systems (Li & Kunieda, 2003). However, no direct, high-resolution imaging data, which could have given more insight or verify these models has yet been published. We have investigated the phase behaviour of an interesting monophasic microemulsion system containing different water concentrations with a constant isooctane/DDAB ratio of 1.5. Previous studies on microemulsion systems containing DDAB with various oils showed unexpected results. As opposed to convention, adding water to those bicontinuous systems showed that they became oil-continuous rather than water-continuous (Chen *et al.*, 1984). This behaviour was explained as a curvature dependent mechanism augmented by oil uptake in the surfactant tail region. Thus the concentration (and type) of the oil is dominant in determining the rather counter-intuitive nanostructural behaviour of the system (Chen *et al.*, 1986). In this case, we did not use liquid ethane at its freezing point as a cryogen, because it dissolves the oil. Isooctane was once again used here for its capability to be vitrified in $LN_2$. We prepared two samples, both with a constant O/S ratio of 1.5, but sample A consisted 20% wt. $H_2O$, whereas sample B was made of 40% wt. $H_2O$. The samples were prepared as previously described, at 25°C in the CEVS chamber, which was saturated with both the oil and water solvents and finally be plunged in $LN_2$. The specimens were coated with a 4 nm Pt/C coating, but not etched, to limit sublimation, which occurred because of the high volatility of isooctane, even at cryogenic temperatures.

A clear bicontinuous morphology can be seen in sample A (Fig. 11), namely, a network of water tubes (swollen inverse thread like micelles) surrounded by the oil as predicted 25 years ago by the model suggested by Ninham and Evans and coworkers (Chen *et al.*, 1986) for this type of bicontinuous system. The diameter of the conduits seen in Fig. 11 is quite uniform, from 30 nm to 40 nm. The holes occasionally seen in between the network (arrows in Fig. 11) are probably domains of isooctane, which had sublimated because of its high vapour pressure. After diluting sample A by water to form sample B, it is evident that inverse swollen micelles were formed, causing the system to become only oil continuous (Fig. 12). These results are again consistent with the data shown by Chen *et al.* (1986). The micelles must be swollen as their sizes (35–45 nm) are too large for being normal micelles and they are very homogenous and small to be considered as vesicles.

*Example #3: 7% wt. dispersion of HiPco carbon nanotubes (CNTs) in a chlorosulphonic superacid.*

We have already shown by cryo-TEM that chlorosulphonic acid is the ultimate solvent for low concentrations of CNTs (CNTs; Parra-Vasquez *et al.*, 2010). However, one needs cryo-SEM to characterize the viscous liquid crystalline phases used as 'dope' for fibre spinning, the liquid crystal domains created by the HiPco multiwalled CNTs (Bachilo *et al.*, 2002) dispersed

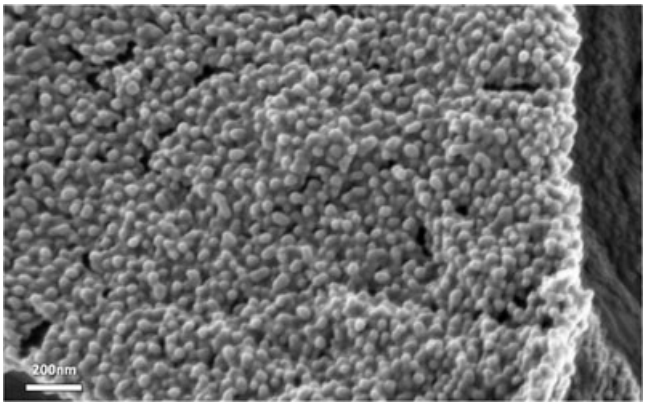


**Fig. 12.** Cryo-SEM image of the microemulsion system of $H_2O$–isooctane–DDAB (O/S = 1.5, $H_2O$ 40% wt.) at 25°C. (a) The image shows an inverse swollen micelle phase present in the specimen bulk. The image was obtained with the InLens detector at WD of 2.8 mm.

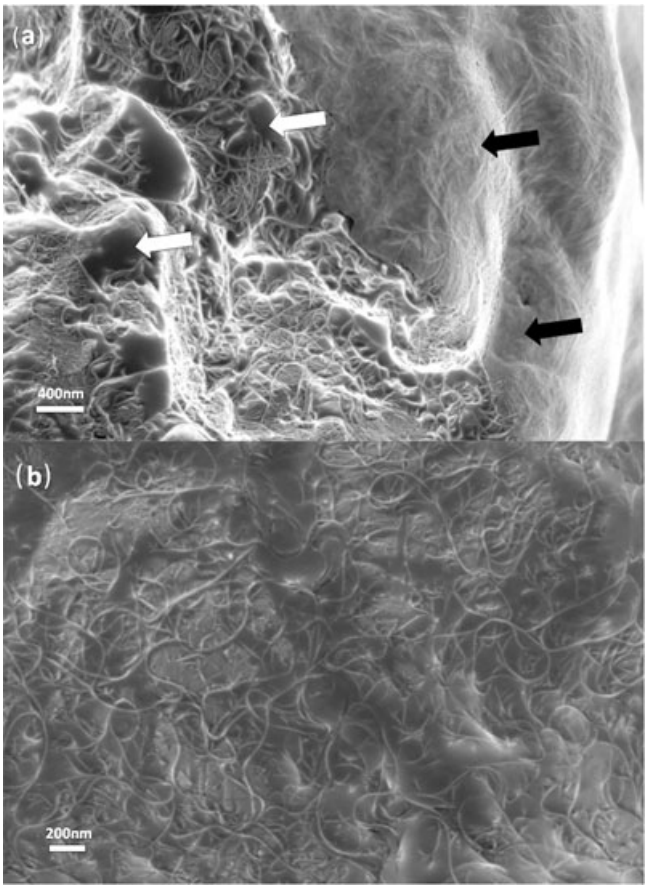


**Fig. 13.** Cryo-SEM images of 7% wt. HiPco MWCNTs dispersed in chlorosulphonic superacid. (a) Image showing partially covered CNTs by their solvent (black arrows) and having solvent in between them (white arrows). The image was obtained with the InLens detector at WD of 3 mm; (b) 'endless strand' (spaghetti-like) morphology is noticeably seen in this image. The images were both obtained with the InLens and SE2 detectors with a mixing ratio of 0.8:0.2 at WD of 2.8 mm.

in the superacid. Chlorosulphonic acid is a highly corrosive and a hygroscopic material, which reacts violently with water to yield sulphuric acid and HCl. Hence, one must work with it in a confined and dry environment. We used the new CEVS to protect the users, while preserving the sample. The specimen was prepared at 25°C while ultrapure dry nitrogen (99.9995%) was purged through the chamber and vented into the hood exhaust. To minimize the sample exposure to ambient humidity, after it was opened, the vial was immediately pushed into the purged CEVS through the chamber's left septa. A fibreglass filter paper was placed on the preparation platform and a glass pipette was used to apply the sample on the planchette. Specimen preparation was carried out gently to avoid acid spillage on the unprotected chamber or tweezers surfaces. After fracturing the specimen, it was not etched because of its low vapour pressure and to avoid acid fumes release.

We imaged a high concentration of CNTs at the fracture surface (Fig. 13). Most CNTs seemed intact, with lengths up to a few microns. It is possible to see that the CNTs are dispersed as individuals in this solvent. This is in agreement with what was shown in recent literature for other types of SWCNTs (Davis *et al.*, 2009). It is also very simple to notice that the chlorosulphonic acid coats some particles and takes the volume in between them (see black and white arrows, respectively, in Fig. 13a). In Fig. 13b an 'endless strand' (spaghetti-like) morphology is seen. This image is similar to a cryo-TEM image taken from an isotropic phase of a more diluted system containing 'carpet-grown' MWCNTs shown by Parra-Vasquez *et al.* (2010) at lower concentrations. Our work is aimed at imaging the liquid crystalline phase that is formed on this system.

The results we show here demonstrate that high-resolution imaging of viscous systems of nanoparticles dispersed in a solvent is possible. This opens an opportunity for direct imaging by EM of systems in their almost natural state never before possible. Up to now, no system for preparing vitrified and fractured specimens can deal with reactive substances. We show that in the case of very reactive samples, using the new CEVS not only helps in preserving their natural state but also allows their safe preparation. As in all three systems given, we obtained consistent results to those shown by other techniques/models, we deduce that by using our methodology, ultrasensitive samples can be prepared under controlled conditions and be imaged by cryo-SEM to give artefact and contamination free results.

**Acknowledgements**

We thank Mr. Moshe Cohen and Mr. Nissim Hodeda of the Chemical Engineering Workshop for their help in planning and building the prototype set of tweezes and Mr. David Haimovich of the HD Engineering Company for developing

the current version. We thank Dr. Ellina Kesselman and Mrs. Na'ama Koifman for their helpful tips in improving the CEVS design and Mrs. Judith Schmidt for her cryo-TEM imaging. We also thank Ms. Olga Kleinerman for preparing the CNTs dispersed in superacid samples, Mrs. Irina Davidovich for preparing the $C_{12}E_5$ microemulsion samples and Mr. Ido Ben-Barak for preparing and imaging the DDAB microemulsion samples. Partial financial support for this work was provided by the Israel Science Foundation (ISF), Grant No. 962/07, by the United States-Israel Binational Science Foundation (BSF), Grant No. 214/2004 and by the Technion-Russell Berrie Nanotechnology Institute (RBNI).

## References

Adrian, M., Dubochet, J., Lepault, J. & McDowall, A.W. (1984) Cryoelectron microscopy of viruses. *Nature* **308,** 32–36.

Bachilo, S.M., Strano, M.S., Kittrell, C., Hauge, R.H., Smalley, R.E. & Weisman, R.B. (2002) Structure-assigned optical spectra of single-walled carbon nanotubes. *Science* **298,** 2361–2366.

Bellare, J.R., Davis, H.T., Scriven, L.E. & Talmon, Y. (1988) Controlled environment vitrification system: an improved sample preparation technique. *J. Electron Microsc. Tech.* **10,** 87–111.

Bellare, J.R., Davis, H.T., Scriven, L.E. & Talmon, Y. (1986) An improved controlled environment vitrification system (CEVS) for cryofixation of hydrated TEM samples. *Proc. 11th Int'l Cong. on Electron Microscopy*, Kyoto, **1,** 367–368.

Chen, S.J., Evans, D.F. & Ninham, B.W. (1984) Properties and structure of three-component ionic microemulsions. *J. Phys. Chem.* **88,** 1631–1634.

Chen, S.J., Evans, D.F., Ninham B.W., Mitchell, D.J., Blum, F.D. & Pickup, S. (1986) Curvature as a determinant of microstructure and microemulsions. *J. Phys. Chem.* **90,** 842–847.

Costello, M.J., Fetter, R. & Corless, J.M. (1982) Optimum conditions for the plunge freezing of sandwiched samples. *Science of Biological Specimens Preparation* (ed. by O. Johari), pp. 105–115 SEM Inc., AMF O'Hare, Chicago, IL.

Danino, D., Gupta, R., Satyavolu, J. & Talmon, Y. (2002) Direct cryogenic-temperature transmission electron microscopy imaging of phospholipid aggregates in soybean oil. *J. Colloid Interface Sci.* **29,** 180–186.

Davis, V.A., Parra-Vasquez A.N. Green, M.J., *et al.* (2009) True solutions of single-walled carbon nanotubes for assembly into macroscopic materials. *Nat. Nanotechnol.* **4,** 830–834.

Echlin, P., Paden, R., Dronzek, B. & Wayte, R. (1970) Scanning electron microscopy of labile biological material maintained under controlled conditions, *Proc. 3rd. Ann. Scanning Electron Microsc. Symp.*, Chicago, IL.

Elder, H.Y., Gray, C.C., Jardine, A.G., Chapman, J.N. & Biddlecombe, W.H. (1982) Optimum conditions for cryoquenching of small tissue blocks in liquid coolants. *J. Microsc.* **126,** 45–61.

Ge, H., Suszynski, W.J., Davis, H.T. & Scriven, L.E. (2007) New controlled environment vitrification system for preparing wet samples for cryo-SEM. *J. Microsc.* **229,** 115–126.

Hisada, A., Yoshida, T., Kubota, S., Nishizawa, N.K. & Furuya, M. (2001) Technical advance: an automated device for cryofixation of specimens of electron microscopy using liquid helium. *Plant Cell Physiol.* **42,** 885–893.

Jahn, W. & Strey, R. (1988) Microstructure of microemulsions by freeze fracture electron microscopy. *J. Phys. Chem.* **92,** 2294–2301.

Jaksch, H., Steigerwald, M. & Drexel, V. (2005) Technologies to characterize nanostructured particles and bulk materials. *Microsc. Microanal.* **11,** 946–947.

Kahlweit, M., Strey, R., Haase, D., *et al.* (1987) How to study microemulsions. *J. Colloid Interface Sci.* **118,** 436–453.

Knoll, G., Oebel, G. & Plattner, H. (1982) A simple sandwich-cryogen-jet procedure with high cooling rates for cryofixation of biological materials in the native state. *Protoplasma* **111,** 161–176.

Koh C. G., Zhang, X., Liu, S., *et al.* (2010) Delivery of antisense oligodeoxyribonucleotide lipopolyplex nanoparticles assembled by microfluidic hydrodynamic focusing. *J. Control Release* **141,** 62–69.

Li, X. F. & Kunieda, H. (2003) Catanionic surfactants: microemulsion formation and solubilization. *Curr. Opin. Colloid Interface Sci.*, **8,** 327–336.

Millazzo, G. (1956) Tensioni di vapore di alcune sostanze organiche a bassa temperatura. *Ann. Chim. (Rome)* **46,** 1105–1111.

Miller, D.D., Bellare, J.R., Evans D.F., Talmon, Y. & Ninham, B.W. (1987) Meaning and structure of amphiphilic phases: inferences from video-enhanced microscopy and cryotransmission electron microscopy. *J. Phys. Chem.* **91,** 674–685.

Moor, H. (1987) Theory and practice of high pressure freezing. *Cryotechniques in Biological Electron Microscopy* (ed. by R.A. Steinbrecht, and K. Zierold), pp. 175–191. Springer-Verlag, Berlin.

Moor, H. & Riehle, U. (1968) Snap-freezing under high pressure: a new fixation technique for freeze-etching. *Proc. 4th Eur. Reg. Conf. Electron Microsc.* **2,** 33–34.

Omer, L., Ruthstein, S., Goldfarb, D. & Talmon Y. (2009) High-resolution cryogenic-electron microscopy reveals details of a hexagonal-to-bicontinuous cubic phase transition in mesoporous silica synthesis. *J. Am. Chem. Soc.* **131,** 12466–12473.

Osumi, M., Konomi, M., Sugawara, T., Takagi, T. & Baba, M. (2006) High-pressure freezing is a powerful tool for visualization of Schizosaccharomyces pombe cells: ultra-low temperature and low-voltage scanning electron microscopy and immunoelectron microscopy. *J. Electron Microsc.* **55,** 75–88.

Parra-Vasquez, A.N., Behabtu, N., Green, M.J. *et al.* (2010) Spontaneous dissolution of ultralong single- and multiwalled carbon nanotubes. *ACS Nano* **4,** 3969–3978.

Shulman, J.H., Stoeckenius, W. & Prince, L.M. (1959) Proposed Microemulsion Basic Structure. *J. Phys. Chem.* **63,** 1677–1680.

Talmon, Y. (1996) Transmission electron microscopy of complex fluids: the state of the art. *Ber. Bunsenges. Phys. Chem.* **100,** 364–372.

Talmon, Y. (2007) Seeing giant micelles by cryogenic-temperature transmission electron microscopy (cryo-TEM). *Giant Micelles: Properties and Applications* (ed. by R. Zana, and E. W. Kaler), 1st edn., pp. 163–177. CRC Press, Boca Raton, FL.

Talmon, Y., Davis, H.T., Scriven, L.E. & Thomas, E.L. (1979) Cold-stage microscopy system for fast frozen liquids. *Rev. Sci. Instrum.* **50,** 698–704.

Taribagil, R.R., Hillmyer, M.A. & Lodge, T.P. (2010) Hydrogels from ABA and ABC triblock polymers. *Macromolecules* **43,** 5396–5404.

Walther, P. (2003) Recent progress in freeze-fracturing of high-pressure frozen samples. *J. Microsc.* **212,** 34–43.

Wandrol, P. (2007) New scintillation detector of backscattered electrons for the low voltage SEM. *J. Microsc.* **227,** 24–29.

Wepf, R., Richter, T., Sattler, M. & Kaech, A. (2004) Improvements for HR- and cryo-SEM by the VCT 100 high-vacuum cryo transfer system and SEM cooling stage. *Microsc. Microanal.* **10**, 970–971.

Zheng, Y., Won, Y.Y., Bates, F.S., Davis, H.T., Scriven, L. E. & Talmon, Y. (1999) Directly resolved core-corona structure of block copolymer micelles by cryo-transmission electron microscopy. *J. Phys. Chem. B* **103**, 1033–1034.

## Supporting Information

Additional Supporting Information may be found in the online version of this article:

In addition to the cryo-SEM imaging done on both samples of the nonionic $C_{12}E_5$ microemulsion system, we also prepared and imaged these samples by cryo-TEM by the methodology shown by Talmon (1996). Although these samples are not ideal for cryo-TEM specimen preparation, we were able to prepare thin enough films and image them by cryo-TEM, hence being the first to acquire cryo-TEM data of this type of microemulsion systems. As seen in Figure S1a, a bicontinuous phase is present in sample A (oil fraction in the water-oil mix, $\alpha = 30\%$ wt., prepared at 31°C). These results are consistent to that shown in Fig. 9 by cryo-SEM. It also can be noticed that the domain dimensions seen in both methodologies are very similar (200–300 nm). The cryo-TEM image of sample B (oil fraction in the water-oil mix, $\alpha = 80\%$ wt., prepared at 37°C) shown in Figure S1(b), shows nanoformations that are reversed swollen-water micelles dispersed in the isooctane continuous phase. That those micelles indeed contain water is seen from that those micelles froze into crystalline ice (see arrows) because of the use of LN2. Moreover, once again, fusion of some micelles that are probably an intermediate aggregate en-route to the bicontinuous phase is observed (arrowheads). The dimensions of the micelles seen here match the ones seen in Fig. 10 (100–200 nm).

**Fig. S1.** Cryo-TEM images of the microemulsion system of $H_2O$-isooctane-7% wt. $C_{12}E_5$. (a) Image of sample A (oil fraction in the water-oil mix, $\alpha = 30\%$ wt. at 31°C), showing a bicontinuous phase. (b) Image of sample B (oil fraction in the water-oil mix, $\alpha = 80\%$ wt. at 37°C) showing reversed swollen-water micelles dispersed in isooctane. In some micelles crystalline ice was formed (see arrows). Note some micelles, which have fused together (arrowheads).

Please note: Willey-Blackwell is not responsible for the content or functionality of any supporting materials supplied by the authors. Any queries (other than missing material) should be directed to the corresponding author for the article.